High-visibility interference fringes with femtosecond laser radiation

Raúl Martínez-Cuenca,[1,2]* Lluís Martínez-León,[1,2] Jesús Lancis,[1,2] Gladys Mínguez-Vega,[1,2] Omel Mendoza-Yero,[1,2] Enrique Tajahuerce,[1,2] Pere Clemente,[2,3] and Pedro Andrés[4]

[1]GROC·UJI, Departament de Física, Universitat Jaume I, 12080 Castelló, Spain.
[2]Institut de Noves Tecnologies de la Imatge (INIT), Universitat Jaume I, 12080 Castelló, Spain.
[3]Servei Central d'Instrumentació Científica (SCIC), Universitat Jaume I, 12080 Castelló, Spain.
[4]Departamento de Óptica, Universitat de València, 46100 Burjassot, Spain.
*rcuenca@fca.uji.es

Abstract: We propose and experimentally demonstrate an interferometer for femtosecond pulses with spectral bandwidth about 100 nm. The scheme is based on a Michelson interferometer with a dispersion compensating module. A diffractive lens serves the purpose of equalizing the optical-path-length difference for a wide range of frequencies. In this way, it is possible to register high-contrast interference fringes with micrometric resolution over the whole area of a commercial CCD sensor for broadband femtosecond pulses.

OCIS Codes: (030.1640) Coherence, (260.3160) Interference, (320.5550) Pulses.

References and Links

1. A. F. Fercher, W. Drexler, C. K. Hitzenberger, and T. Lasser, "Optical coherence tomography-principles and applications," Rep. Prog. Phys. **66**(2), 239–303 (2003).
2. L. Vabre, A. Dubois, and A. C. Boccara, "Thermal-light full-field optical coherence tomography," Opt. Lett. **27**(7), 530–532 (2002).
3. E. Cuche, P. Poscio, and C. Depeursinge, "Optical tomography by means of a numerical low-coherence holographic technique," J. Opt. **28**(6), 260–264 (1997).
4. L. Martínez-León, G. Pedrini, and W. Osten, "Applications of short-coherence digital holography in microscopy," Appl. Opt. **44**(19), 3977–3984 (2005).
5. P. Massatsch, F. Charrière, E. Cuche, P. Marquet, and C. D. Depeursinge, "Time-domain optical coherence tomography with digital holographic microscopy," Appl. Opt. **44**(10), 1806–1812 (2005).
6. A. A. Maznev, T. F. Crimmins, and K. A. Nelson, "How to make femtosecond pulses overlap," Opt. Lett. **23**(17), 1378–1380 (1998).
7. Z. Ansari, Y. Gu, M. Tziraki, R. Jones, P. M. W. French, D. D. Nolte, and M. R. Melloch, "Elimination of beam walk-off in low-coherence off-axis photorefractive holography," Opt. Lett. **26**(6), 334–336 (2001).
8. B. E. A. Saleh, and M. C. Teich, *Fundamentals of Photonics*, 2nd ed. (Wiley, 2007), Chap. 11.
9. E. N. Leith, and G. J. Swanson, "Achromatic interferometers for white-light optical processing and holography," Appl. Opt. **19**, 638–644 (1980).
10. J. Hebling, I. Z. Kozma, and J. Kuhl, "Compact high-aperture optical setup for excitation of dynamic gratings by ultrashort light pulses," J. Opt. Soc. Am. B **17**(10), 1803–1805 (2000).
11. T. Brabec, and F. Krausz, "Nonlinear optical pulse propagation in the single-cycle regime," Phys. Rev. Lett. **78**(17), 3282–3285 (1997).
12. H. Xiao, and K. E. Oughstun, "Failure of the group-velocity description for ultrawideband pulse propagation in causally dispersive, absorptive dielectric," J. Opt. Soc. Am. B **16**(10), 1773–1785 (1999).
13. P. Andrés, J. Lancis, E. E. Sicre, and E. Bonet, "Achromatic Fresnel diffraction patterns," Opt. Commun. **104**(1-3), 39–45 (1993).
14. J. Lancis, E. E. Sicre, A. Pons, and G. Saavedra, "Achromatic white-light self-imaging phenomenon-an approach using the Wigner distribution function," J. Mod. Opt. **42**(2), 425–434 (1995).
15. G. Mínguez-Vega, O. Mendoza-Yero, M. Fernández-Alonso, P. Andrés, V. Climent, and J. Lancis, "Experimental generation of high-contrast Talbot images with an ultrashort laser pulse," Opt. Commun. **281**, 374–379 (2008).

1. Introduction

Femtosecond light sources provide a valuable tool for three-dimensional ranging through coherence gating. Depth resolution is controlled by the spectral bandwidth of the pulse through the equation $2\lambda_o^2 \ln 2 / \pi\Delta\lambda$ [1], with λ_o and $\Delta\lambda$ the center wavelength and the bandwidth of the source respectively. Optical coherence tomography (OCT) takes advantage of low-coherence interferometry to provide cross-section images of biological tissue. OCT images can be recorded either point by point through a fast two-dimensional scanning system or using wide-field techniques, which provide en-face *(XY)* tomographic images without transverse scanning [2].

Short-coherence digital holographic microscopy was proposed by Cuche et al in 1997 as a new wide-field tomographic modality [3]. Here, an off-axis hologram results from the interference between an object wave scattered by the sample and a reference wave in a Michelson-type interferometer. The hologram is recorded onto a CCD camera allowing digital reconstruction. When a low-coherence source is used to record the hologram it is possible to perform tomography of the sample [4].

An axial resolution of 11 μm has been demonstrated with a 80 fs pulsed laser source [5]. As noted by the authors, no further improvement in axial resolution is expected by reducing the pulse width as the bandwidth of the source must be kept small enough to preserve the formation of fringes to record the hologram. The point is the so-called walk-off effect [6,7]. Using a temporal picture, the reduced coherence length restricts interference fringes to a diamond-shaped region with size proportional to the coherence time, roughly the inverse of the spectral bandwidth. From a spectral point of view, fringes are washed-out as each spectral component generates its own fringe pattern but with a different period. Anyway, the number of recordable fringes is given by $\lambda_o / \Delta\lambda$ [8] which, for instance, for a femtosecond laser delivering 10 fs pulses at a carrier wavelength of 800 nm is only 9. This fact leads to a reduced field of view for holographic reconstruction.

Inspired by the achromatic grating interferometer [9], this problem was addressed by the use of a diffraction grating as a beam splitter [6]. Pulse front tilt originated at the grating forces pulses to overlap over the whole diameter of the beam. This smart approach has been extensively employed for transient grating experiments [10] but it lacks the flexibility necessary for holographic recording and tomographic measurement. Pulse front tilt has also been performed by the use of specific-purpose prisms in the two arms of a Michelson-type interferometer leading to an increased number of fringes for the off-axis geometry [7].

Here, we propose a new pulse front tilt mechanism in a Michelson interferometer that is fully compatible with holographic applications. The key is an easy-implemented dispersion compensating module (DCM) constituted by a diffractive lens located outside the interferometer. The device is designed to equalize the optical path length with frequency just to get a nearly zero differential group delay between the object and the reference beam for all the spectral components when the two arms of the interferometer have an identical length. This link guarantees a flat visibility, nearly unity, for the interference fringes along a considerable region of the beam. Optical path equalization is performed through the dispersion introduced by diffractive lenses. For 10 fs pulses at a wavelength carrier of about 800 nm, results of computer simulations and laboratory experiments demonstrate an enhancement in the number of recordable fringes by a factor of about 36.

2. Frequency-domain analysis of interference of short pulses traveling through dispersive media

Let us consider a pulsed plane wave with carrier angular frequency ω_o, $a(t - z/c)e^{i\omega_o(t-z/c)}$, traveling along a dispersive medium in the direction indicated by the z-axis. The pulse carries

a total intensity $I_o = \int |a(\tau)|^2\, d\tau$, with $\tau = t - z/c$, and we denote by $S(\omega)$ the baseband spectral energy distribution of the pulse. In mathematical terms,

$$S(\omega) = \left| \tilde{a}(\omega) \right|^2 = \left| \int_{-\infty}^{\infty} a(t) e^{-i\omega t}\, dt \right|^2, \tag{1}$$

with $\tilde{a}(\omega)$ the Fourier transform of the pulse envelope $a(t)$. The superposition of the pulse with a time-delayed and a spatially tilted replica of itself can be implemented with the help of a Michelson interferometer. When the pulses overlap, for slow detection compared with the pulse duration, the time-integrated intensity of their sum is

$$I = I_o + \mathfrak{Re} \left\{ \int_{-\infty}^{\infty} S(\omega) e^{i\Delta\Phi(\omega+\omega_o)} d\omega \right\}, \tag{2}$$

where Re designs the real part and $\Delta\Phi(\omega + \omega_o)$ is the phase difference between the object and the reference pulse for the spectral component with frequency $(\omega + \omega_o)$ at the superposition point.

A further insight into the problem can be gained if $\Delta\Phi(\omega + \omega_o)$ is expanded around the carrier frequency up to second order as

$$\Delta\Phi(\omega + \omega_o) \simeq \Delta\Phi_o + \tau\,\omega + \frac{1}{2}\tau'\,\omega^2, \tag{3}$$

where τ and τ' are the first-order and second-order derivatives of the phase difference with respect to frequency and evaluated at the carrier frequency. The above quantities are identified as the differential group delay (DGD) and the differential group delay dispersion (DGDD) between the object and the reference waves for ω_o. We assume the slowly varying envelope approximation and the Taylor series expansion of the phase to be valid. The above assumptions set the ultimate limit for the maximum bandwidth of $S(\omega)$ which, in turn, leads to pulse duration of a few cycles of the optical carrier [11]. Also, Taylor series expansion is not adequate for causally dispersive, absorptive dielectrics when the propagation distance exceeds a characteristic absorption depth setting the limit for the penetration depth in tomographic applications [12]. Anyway, experimental results in Section 4 validate the goodness of the above assumptions. Inserting Eq. (3) into Eq. (2) we find

$$I(\tau, \tau') = I_o \left\{ 1 + V(\tau, \tau') \cos\left[\Delta\Phi_o + \varphi(\tau, \tau') \right] \right\}, \tag{4}$$

where $V(\tau, \tau') = \left| \gamma_g(\tau, \tau') \right|$ and $\varphi(\tau, \tau') = \arg\left(\gamma_g(\tau, \tau') \right)$ with

$$\gamma_g(\tau, \tau') = \frac{1}{I_o} \int_{-\infty}^{\infty} S(\omega) e^{i\tau\omega}\, e^{i(\tau'/2)\omega^2}\, d\omega. \tag{5}$$
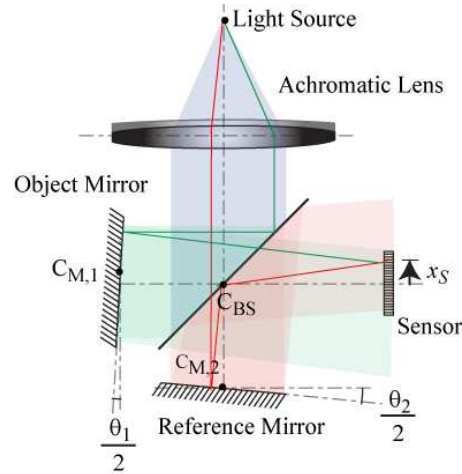
Fig. 1. Sketch of a conventional Michelson interferometer with tilted mirrors for spatial record-ing of interference fringes. The length mismatch between the interferometer arms is $\Delta e \equiv C_{BS}C_{M,1} - C_{BS}C_{M,2}$. The carrier frequency and the spectral width of the source fix the number of recordable fringes.

It is thus apparent that the ability of the pulse to interfere with a delayed replica of itself is governed by a generalized complex degree of temporal coherence $\gamma_g\left(\tau,\tau'\right)$ that accounts for the presence of dispersion within the interferometric setup.

When no dispersion is present, or the DGDD is set to zero, we recover the well-established Wiener-Khintchine theorem. This result states that the complex degree of temporal coherence and the spectral energy distribution are linked through a Fourier transform relationship. The most common situation corresponds to free-space propagation after the beam splitter (see Fig. 1). For this case, the value of the phase difference is determined by the length mismatch be-tween the interferometer arms (Δe) and the mirror tilts θ_1 and θ_2 through the expression $\Delta\Phi(\omega)$ = $[2\Delta e + x_S\,(sin\theta_2 - sin\theta_1)]\,\omega/c$. In the above expression c denotes the speed of light and x_S the transverse coordinate at the sensor plane. Note that $\Delta\Phi(\omega)$ is linear with frequency so that $\tau' = 0$. The two usual cases $\theta_1 = \theta_2$ and $\Delta e = 0$ can be obtained from the above result. For the inter-ference of parallel plane waves, we recover the interferogram trace $I(x_S) = I_o\left[1 + V(\tau)\cos\left(\tau\omega_o + \varphi(\tau)\right)\right]$, with $\tau = 2\Delta e/c$. Also, the same trace holds when $\theta_1 \neq \theta_2$ and $\Delta e = 0$ but now the interference pattern is codified in the tranverse coordinate x_S at the output plane through the relationship $\tau = x_S\,(sin\theta_2 - sin\theta_1)/c$.

As a matter of fact, for a pulse with Gaussian spectrum the visibility, defined in the usual way $V = \left(I_{\max} - I_{\min}\right)/\left(I_{\max} + I_{\min}\right)$, is also a Gaussian function. The number of observable fringes is controlled by the coherence time, the width of the complex degree of coherence, and, for the Gaussian situation, is of the order of $\omega_o\,/\Delta\omega = \lambda_o\,/\Delta\lambda$ with $\Delta\omega$ the spectral width [8]. Also the transverse position of the central fringe with the length mismatch is given by $x_S = 2\Delta e/(sin\theta_2 - sin\theta_1)$ which accounts for the walk-off effect.

The dispersion introduced by the optical materials employed in the setting of the interfe-rometer increases the pulse duration at the interference region. We assume perfect antireflec-tion coatings for the whole spectrum of the pulse and that no-absorption bands of the materials are present so frequency-dependent lossy effects are neglected [12]. Effects of dispersion are modelled through a chirp filter in the spectral domain and, then, the baseband spectrum of the incoming stretched pulse reads as $\tilde{a}_d\left(\omega\right) = \tilde{a}\left(\omega\right)\exp\left(i\Psi_d''\,\omega^2\right)$, where the parameter Ψ_d'' accounts for dispersion introduced by the glass in both the lens and the beam-splitter. Note

that both reference and object beams suffer from the same time broadening so no relative additional phase difference is introduced, which guarantees validity of Eq. (2). The time-integrated interferometric trace computes the autocorrelation signal for the input field and, thus, it is only sensible to the spectral energy distribution. In other words, due to the phase-only filtering nature of the dispersive effect $\left|\tilde{a}_d\left(\omega\right)\right|^2 = \left|\tilde{a}\left(\omega\right)\right|^2$ and the interferometric signal in Eq. (2) is independent of the value of the dispersion parameter Ψ''_d. For the case of frequency-dependent absorption a further visibility reduction is expected due to the narrowing of the effective spectral energy density.

We emphasize, however, that pulse broadening reduces the temporal resolution of the interferometric signal in the case that a time-resolved detection scheme (FROG, SPIDER, …) is employed. In the case temporal resolution of the interferometric fringes is of interest, as for transient-grating spectrometry, a conventional pre-chirping unit can be used at the exit of the laser system so that the pulse at the output plane results in a transform-limited signal which ensures maximum temporal resolution.

Interestingly, our approach can be easily applied in a different context to explain the formation of broadband interference fringes with unit visibility in the achromatic grating interferometer [6]. Usually, the symmetric configuration corresponding to the interference between diffraction orders $+ 1$ and -1 is considered. Here a wavelength independent phase difference $\Delta\Phi(\omega_o) = 4\pi x_S /d$, with d the grating period, is achieved. In this way, $\tau = 0$ and $\tau' = 0$. This results in a pure cosenoidal interferogram with no fringe modulation $I(x_S) = I_o\left[1 + \cos\left(2\pi x_S /p\right)\right]$ and period p = d/2.

3. Optical setup design

We consider the use of a diffractive lens after beam recombination in the beam splitter to equalize the phase difference with frequency at the output plane (see Fig. 2). We assume paraxial approximation and $\Delta e = 0$. Here, we take advantage of the inherent dispersive nature of diffractive optical elements to perform frequency equalization of the optical path length difference (OPLD). Specifically we recall that the focal length $Z(\omega)$ of a diffractive lens is a linear function of the wave frequency; i.e., $Z(\omega) = Z_o \omega/\omega_o$, where Z_o denotes the focal length for the carrier ω_o. For this case, the value of the phase difference is given by
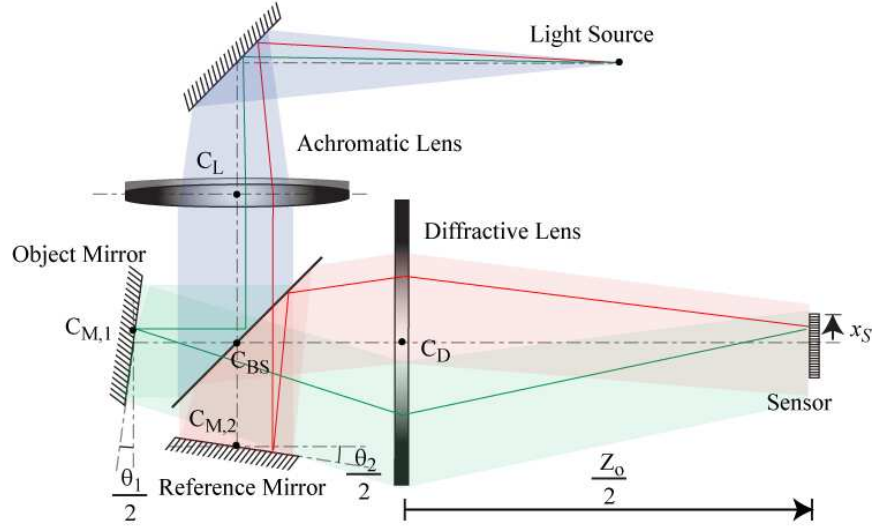
Fig. 2. Interferometer for femtosecond pulses with extended visibility. The arms of the interferometer are of identical length and a diffractive lens is inserted at the image focal plane of the achromatic lens.

$$\Delta\Phi(\omega) = \frac{\omega\,\Delta L(\omega)}{c},\tag{6}$$

where the frequency-dependent OPLD, $\Delta L(\omega)$ is evaluated as

$$\Delta L(\omega) = \frac{f}{2B}\Big[Af\left(\theta_2^2 - \theta_1^2\right) - 2x_S\left(\theta_2 - \theta_1\right)\Big].\tag{7}$$

In the above equation the symbols A and B stand for first-row elements of the paraxial ABCD matrix between the source and the observation planes which, indeed, are wavelength dependent. Again, x_S denotes transverse coordinate at the sensor and f is the focal length of the achromatic objective.

Ideally, $\Delta\Phi(\omega)$ should be independent on the frequency. This situation cannot be satisfied for the optical setup in Fig. 2. However, geometrical parameters can be tuned in order to minimize the above functional dependence. To this end, we impose the first-order condition $\tau = 0$. In a temporal picture, we require an identical arrival-time over the whole output plane for the wave packets traveling through the reference and the object arms of the interferometer. As a result, a high visibility for the interferential fringes at the output is expected. By virtue of Eqs. (6) and (7), OPLD equalization leads to the constraints

$$\frac{\partial}{\partial\omega}\left(\frac{\omega}{B}\right)\bigg|_{\omega_o} = 0, \quad \frac{\partial}{\partial\omega}\left(\frac{A\omega}{B}\right)\bigg|_{\omega_o} = 0.\tag{8}$$

To fulfill the above two conditions interference fringes must be recorded at a distance $Z_o/2$ from the diffractive lens which, in turn, must be located at the image focal plane of the achromatic objective. Under the above restrictions, and neglecting the effect of higher-order dispersion terms, we get a unit-visibility interferometric trace with spatial period p = $\pi c/(\theta_2-\theta_1)\omega_o$. We recognize that this equalizing optical device is closely related to the continuous-wave white-light Fresnel transformer reported in [13], [14] and [15].

We have developed a first-order theory. So a residual modulation for the interference fringes is expected. The fringe envelope is evaluated through Eq. (5) with $\tau = 0$ and $\tau' =$

$\Delta\Phi_o/\omega_o^2$ where $\Delta\Phi_o$ is given by Eq. (6) for $\omega = \omega_o$ after the conditions derived in Eq. (8) are substituted into matrix elements A and B. Also, the value for τ' is derived from the second derivative of Eq. (6) with achromatic compensation. Note that Eq. (5) indicates that the Fourier transform relation between the complex degree of coherence and the spectral energy is substituted by a Fresnel transformation. It is one of the main results of our work as it is the only way the optical design in Fig. 2 can be carried out. In Fig. 3 we plot the visibility function $V(x_S)$ for the interferograms at the sensor for the optical setups in Fig. 1 (solid curve) and 2 (dashed curves) as a function of the normalized sensor coordinate x_S/p. We assume a Gaussian spectrum centered at ω_o and full-width-at-half-maximum (FWHM) width $\Delta\omega$. For the plot, we choose $\omega_o = 2.40\ 10^{14}\ Hz$ and $\Delta\omega = 2.44\ 10^{13}\ Hz$ (i.e., $\lambda_o = 789$ nm and $\Delta\lambda = 81.6$ nm). It appears that the diffractive lens enhances the sensor region over which interference fringes are observable by at least an order of magnitude. In fact, it can be demonstrated that the gain factor, defined as the ratio between the FWHM width of the function $V(x_S)$ for the interference fringes obtained with the Michelson interferometer with and without DCM, respectively, is given by $15^{1/2}\omega_o/\Delta\omega$. Note that this is a theoretical value that provides the increment in the number of recordable fringes, which is entirely determined by the characteristics (carrier frequency and spectral width) of the pulse. For the present numerical example the gain factor is of about 36. From the point of view of laboratory results, this theoretical number is slightly reduced due to the effect of higher-order terms in the expansion of $\Delta\Phi(\omega + \omega_o)$ *and the presence of spatial variations in the input femtosecond beam*. To take into account this effect, we test the goodness of the quadratic approximation in Eq. (3) in the same plot. To this end, visibility is evaluated directly through Eq. (2). Now, the full ω–dependence of the OPLD is retained for the calculation. Results are plotted in short-dashed line. Only a slight deviation is observed for a sensor area covering a huge amount of fringe periods.
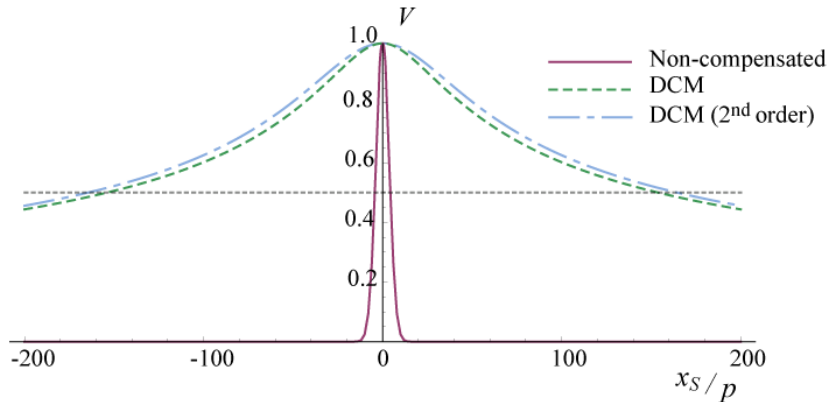

Fig. 3. Plot of the visibility of the interference fringes as a function of the normalized transverse coordinate at the sensor plane for the optical setup in Fig. 1 (solid line) and the optical setup in Fig. 2. For the former, both the quadratic approximation (long-dashed line) and the full dependence with the frequency of the phase difference between the object and the reference wave (short-dashed line) are plotted.

4. Experimental results

We proved the feasibility of our diffractive-lens based DCM through laboratory experiments. A picture of the optical setup is shown in Fig. 4.a). In the right lower corner of the picture we see the spatial filter and the collimating lens to create the pulsed plane-wave. The achromatic lens (AL), beam splitter (BS), two-mirrors (M1 and M2), the diffractive lens (DL), and the CCD sensor are labeled in the picture. We used a nearly Gaussian pulse from a commercial Ti:sapphire laser oscillator. The laser system delivers 9 nJ pulses at 75 MHz repetition rate. In

Fig. 4.b) the spectrum of the pulse (solid curve) together with its Gaussian fit (dashed curve) are plotted. Spectrum parameters ω_o and $\Delta\omega$ are those used for the plot in Fig. 3. Normally, the pulses are transform-limited to roughly 10 fs. However, the pulse can be pre-chirped so that at the sensor results in a transform-limited signal to increase temporal resolution of the interference as explained in Section 2. Fringes were captured by a CCD camera with a pixel size of 6 μm and a sensor area of 7.68×6.14 mm^2. The focal lengths for the refractive achromatic objective f and the diffractive lens Z_o were chosen as 200 mm and 143 mm, respectively. The diffractive lens was located at the image focal plane of the objective and the sensor was positioned 71.5 mm from the dispersive component. All the above parameters were chosen just to meet achromatic requirements specified through Eq. (8).
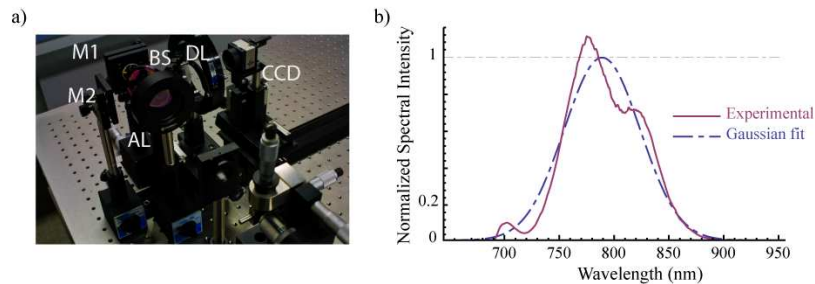

Fig. 4. a) Picture of the interferometer with the DCM for femtosecond pulses. b) Spectral energy distribution of the Ti:sapphire femtosecond source (solid line) and its Gaussian fit (dashed line).

Figure 5 shows the interference fringes and the corresponding line scans showing the depth of fringe modulation recorded as a function of the sensor coordinate without (a) and with the DCM (b). For both pictures, fringe spacing is identical (p = 42 μm). This is accomplished by changing slightly the relative angle between the mirrors for the optical setups in Figs. 1 and 2. Interference visibility nicely fits the theoretical predictions shown in Fig. 3 for both situations. Note the significant improvement in the number of recordable fringes (by 240 in the picture). For the DCM situation they cover the whole sensor area keeping a visibility higher than 0.5. As noted previously, the slightly reduction with respect to the theoretical value of 36 is mainly due to the effect of higher-order terms in the expansion of $\Delta\Phi(\omega + \omega_o)$ *and the presence of spatial variations in the input femtosecond beam.*

5. Conclusions

High-visibility interference fringes with broad bandwidth femtosecond pulses are recorded by means of a modified Michelson interferometer. The device incorporates a diffractive lens to equalize the optical path length difference between the object and the reference wave with frequency. In this way, the width of the visibility function, measured as its FWHM, in terms of the normalized coordinate x_S/p is increased by a factor $15^{1/2}\omega_o/\Delta\omega$ with respect to the non-equalized situation. We have experimentally recorded interference fringes with 42 μm spacing over the whole sensor area of a commercial CCD camera. A net gain of at least 30 for the the number of recordable fringes (visibility higher than 0.5) is achieved for a commercial Ti:sapphire femtosecond laser oscillator delivering 10 fs pulses at 800 nm.
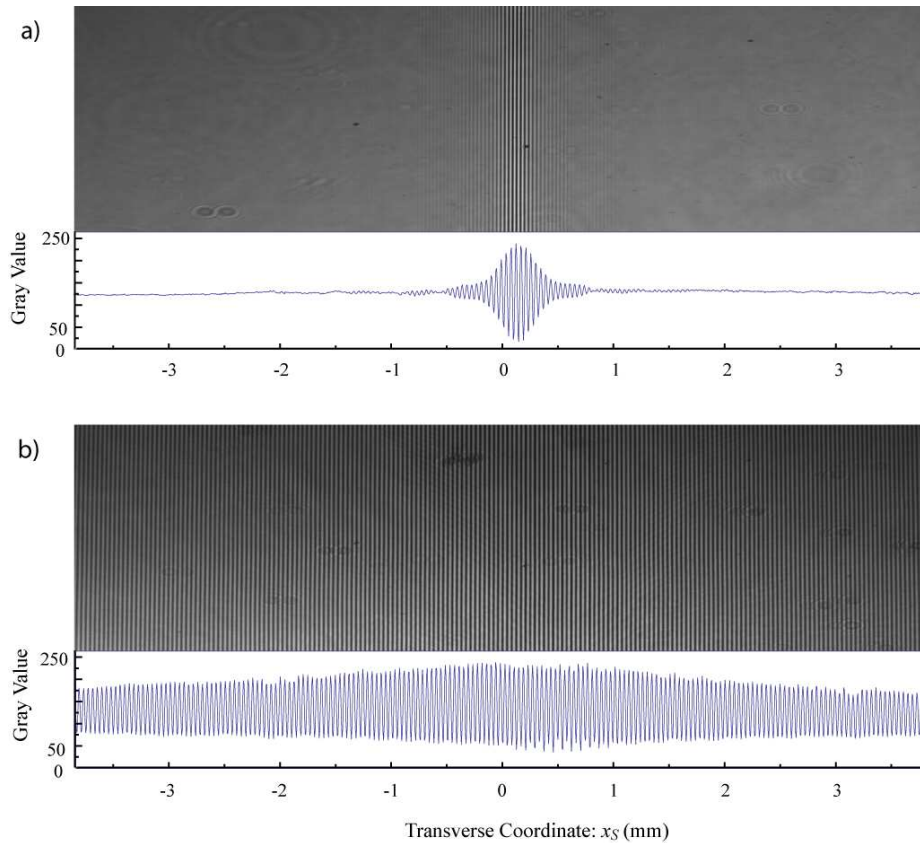
Fig. 5. Interference fringes and corresponding line scans recorded at the sensor plane of: (a) the optical setup in Fig. 1; and (b) the optical setup in Fig. 2.